Real-time dynamics of clusters. II. I_2X_n ($n=1$; X=He, Ne, and H_2), picosecond fragmentation

M. Gutmann,[a] D. M. Willberg, and A. H. Zewail
Arthur Amos Noyes Laboratory of Chemical Physics,[b] California Institute of Technology, Pasadena, California 91125

(Received 1 July 1992; accepted 25 August 1992)

In this second paper (II) of a series, we report our picosecond time-resolved studies of the state-to-state rates of vibrational predissociation in iodine–rare gas (van der Waals) clusters. Particular focus is on the simplest system, I_2He, which serves as a benchmark for theoretical modeling. Comparisons with I_2Ne and I_2H_2 are also presented. The results from measurements made in real time are compared with those deduced from linewidth measurements, representing a rare example of a system studied by both methods under identical conditions and excited to the same quantum (v_i') states. The discrepancies are discussed in relation to the origin of the broadening and preparation of the state. The rates as a function of v_i' display a nonlinear behavior which is examined in relation to the energy-gap law. The measured absolute rates and their dependence on v_i' are compared with numerous calculations invoking classical, quantum, and semiclassical theories. In the following paper (III in this series), the cluster size of the same system, I_2X_n, is increased ($n=2$–4) and the dynamics are studied.

I. INTRODUCTION

The first paper[1] in this series, henceforth referred to as (I), presented our picosecond time-resolved studies of the dynamics of I_2Ne and I_2Ar clusters. In this paper, new studies on the I_2He system are presented, as well as on the I_2H_2 and I_2Ne systems. Here, as in (I), the primary goal of these studies is to understand the dynamics of intramolecular vibrational-energy redistribution (IVR) and vibrational predissociation (VP) within these clusters. For the simplest case, I_2X_n ($n=1$), the state-to-state rates of the reaction describe the following process:

$$I_2^*X(v_i') \xrightarrow{k(v_i';v_f')} I_2^*(v_f')+X, \qquad (1)$$

which is VP from the bound I_2 stretch (v_i' quantum number) potential to the translational continuum of the I_2 and X motion. The asterisk denotes the excited electronic state B, and X=He, Ne, Ar, or H_2, all with $n=1$. In the following paper, we present our study for I_2X_n with $n=2$–4.

The experiments are performed using the picosecond pump–probe/molecular beam methodology.[2] The initial picosecond pump pulse prepares the cluster in a specific initial $B(v_i')$ quantum state of the complex. This is followed by energy transfer out of the iodine stretching motion into the van der Waals modes, resulting in the fragmentation of the cluster. The picosecond probe pulse detects the nascent I_2 in its final $B(v_f')$ vibronic state. For the cases of I_2He and I_2Ne, the energy of one quantum of the I_2 stretch mode exceeds the van der Waals binding energy, and the final I_2 fragment is liberated with $v_f' = v_i' - 1$. The excess energy is converted into translational kinetic energy of the fragments and excitation of the rotational levels of the nascent I_2.

The measured rise of I_2 fragments in v_f' directly gives the state-to-state rate of VP. Since these rates are measured over a wide range of the initial quantum number v_i', a number of theoretical models can be tested for their prediction of the absolute rates and their dependence on v_i'. The work on the I_2He system was performed with two primary objectives in mind. First, in the extensive and pioneering spectroscopic work[3] it was found that I_2He is the best characterized of all the I_2X clusters. The rotational structure of the complex was resolved and Levy and coworkers were able to obtain both the structure[4] of the complex and the linewidths.[5] From the linewidth measurements, assuming homogeneous broadenings, they deduced VP lifetimes[5] over the same range of v_i' levels that we are able to measure in real time. Therefore, I_2He is an ideal system for comparison of the VP lifetimes obtained by frequency- and time-resolved methods.

Second, the I_2He results and those of the I_2Ne system provide two independent and calibrated sets of data which allow comparison with theoretical models of VP for the effects of mass and energy. The majority of these theoretical studies, including a quantum mechanical treatment of VP for a nonlinear configuration, have focused on the I_2He system.

For example, the "energy-gap" model of Beswick and Jortner[6] identifies the energy difference between the van der Waals bond energy and the spacing between vibrational levels of the I_2 stretch as the key factor controlling the VP rate. The evidence from previous studies indicates that I_2He and I_2Ne clusters have similar structures, i.e., "T" shaped, and that both decay via one primary channel (unlike I_2Ar which undergoes electronic as well as vibrational predissociation). Therefore, in comparing the VP rates of I_2He and I_2Ne, aside from the He/Ne mass ratio, the major difference should be in their respective van der Waals potential well depths. Below, we shall consider this and other theories.

[a] Deutsche Forschungsgemeinschaft post-doctoral fellow from Germany.
[b] Contribution number 8638.

The paper is organized as follows: In Sec. II the experimental methodology is described, and in Sec. III the results are presented. In Sec. IV we discuss the dynamics and examine classical and quantum mechanical theories; concluding remarks are presented in Sec. V.

II. EXPERIMENT

The experiments were performed using a combination of picosecond laser and molecular beam techniques. Detailed descriptions of the experimental methodology and apparatus were presented in (I) and will not be given here. In the following, we give a brief summary and discuss the additional experimental conditions which are relevant to the present study.

As in (I), two color picosecond pulses were combined in a pump–probe configuration using a Michelson interferometer. The pump and probe beams were spatially overlapped on a dichroic beam splitter and then gently focused (100 cm lens) to intersect the expansion 19 mm ($X/D = 125$) downstream from the nozzle. The probe was tuned to the $f \leftarrow B(v_f')$ transition of the nascent I_2. Ultraviolet fluorescence from the ion-pair f state was detected and measured as a function of the time delay between the pump and probe pulses. For the purpose of calibration, prior to the measurement of VP, we tuned the pump laser to the corresponding bare iodine $B(v_f') \leftarrow X(v'' = 0)$ transition while keeping the probe laser the same for the $f \leftarrow B(v_f')$ transition. This helped establish the overlap of the pump and probe pulses in both time and space, and set the proper conditions for probing nascent I_2. Temporal resolution in experiments of this nature is limited only by the cross correlation between the pump and probe laser pulses. For the experiments reported here, the cross correlations were approximately Gaussian in profile and the FWHM values were typically 40 ± 3 ps.

The molecular beam apparatus consisted of three chambers: the source, buffer, and a time-of-flight compartment, each pumped seperately by diffusion pumps. For the I_2Ne and I_2Ar experiments, both a cw glass nozzle (nozzle diameter: 75 μm) and a pulsed solenoid valve (150 μm diameter; General Valve series 9) were used. The cw glass nozzle allowed us to take full advantage of the high repetition rate (up to 800 Hz) of our modelocked/Q-switched laser system, while with the pulsed valve, we were restricted to repetition rates of 100 Hz. In order to enhance I_2He and I_2H_2 cluster formation in the molecular beam, high backing pressures (up to 160 psig) were required and the pulsed nozzle was used exclusively. The various clusters studied in this set of experiments, I_2He, I_2Ne, I_2Ar, and I_2H_2, were all formed in free-jet expansions of helium (99.997% purity, Liquid Air), or neon (99.996% purity, Spectra Gases Inc.) with iodine (99.999% purity, Aldrich) seeded at room temperature vapor pressure. In the case of I_2He and I_2Ne clusters, neat helium or neon was used as the carrier gas. Stagnation pressures for the I_2Ne experiments were typically 60 psig, while for the I_2He experiments they were 130–160 psig. [For I_2Ar see (I)]. The I_2H_2 experiments were performed with a mixture of $\sim 3\%$ H_2 in helium at a stagnation pressure of approximately 160 psig. The ratio for these mixtures was chosen to maximize the cluster signal.

Selective excitation of the desired cluster was extremely important as the expansion contained both bare iodine and the larger I_2X_n clusters. The spectroscopic studies of Levy and co-workers[3] proved invaluable in this regard. It was shown that for the I_2Ne_n clusters, where $n < 7$, the $B(v') \leftarrow X(v''=0)$ transition is blueshifted ($n \times 6.65$ cm^{-1}) from the corresponding bare I_2 transition. For I_2He_n clusters the blueshift was shown to be $n \times 3.78$ cm^{-1}.

The picosecond lasers used in the experiments had a bandwidth of 3 cm^{-1}, thus it was possible to tune the pump laser to selectively excite a given cluster to a given $B(v_i')$ vibronic state. However, since the blueshift for the I_2He cluster is only 3.78 cm^{-1}, one may expect the "tail" of the pump laser to overlap the bare iodine $B(v_i') \leftarrow X(v'' = 0)$ transition. A difficulty would arise as the probe laser could, in principle, excite transitions from both the "incidental" bare iodine in the v_i' vibronic state and the nascent iodine in the v_f' state (produced by VP). Thus the I_2He (v_i') transient could be contaminated with bare I_2 (v_i') signal. To test for such contributions, the experiment was repeated for every I_2He (v_i') level under identical conditions, except that the pure He was replaced by pure Ne in the expansion. If there was bare I_2 signal contamination in the transient, then it would be expected that the signal be indifferent to which of the two gases was used in the expansion. Since these test experiments showed no signal when He was replaced by Ne, we were confident of the integrity of the observed I_2He transients.

Another possible difficulty could arise because the transitions for I_2He and I_2Ne for a given v' are only 2.87 cm^{-1} apart. Given the bandwidth of the laser, it is possible to excite one species transition while tuned to the maximum of the other. However, since only neat helium or neon were used, this contamination of transitions is not a problem.

III. RESULTS

The state-to-state lifetimes and rates for the I_2Ne and I_2Ar systems have been presented in (I) and are listed in Table I for comparison with the new results for the I_2He system. Figure 1 shows a typical transient for I_2He and Fig. 2 shows transients of the I_2He and I_2Ne system for the quantum number $v_i' = 22$. The time constants (τ) were determined by fitting the transients to an exponential rise convoluted with a Gaussian system response function. The fitting procedure was based on a Marquardt nonlinear least-squares fitting routine.[7] For all the transients reported, no parameters were fixed other than the cross-correlation bandwidth. For some of the transients, especially for the low v_i' values which required longer scans, a baseline slope factor was included in the fits. For both the I_2He and the I_2Ne fits, the zero of time was consistent with those obtained from bare I_2 control scans; there is no evidence of an induction period within the time resolution of our experiments. The measured values of τ for I_2He as a

TABLE I. The measured (in real-time) state-to-state rates and lifetimes for the I_2He and the I_2Ne systems.[a]

v_i'	I_2He τ (ps)	I_2He VP rate ($\times 10^9$ s^{-1})	I_2Ne τ (ps)	I_2Ne VP rate ($\times 10^9$ s^{-1})
13			216±16	4.6±0.4
14			196±12	5.1±0.3
15			182±20	5.5±0.6
16			160±15	6.3±0.6
17	128±2	7.8±0.2	126±12	7.9±0.8
18	115±9	8.7±0.7	107± 9	9.3±0.9
19	101±4	9.9±0.4	87± 4	11.5±0.9
20	94±4	10.6±0.5	78± 4	12.8±1.0
21	82±4	12.2±0.6	69± 6	14.5±0.7
22	75±6	13.3±1.0	58± 3	17.2±0.9
23	65±5	15.6±1.2	53± 3	18.9±1.0

[a]In this table, the reported errors represent one standard deviation for a number of independent measurements.

function of v_i' are shown in Fig. 3 (and listed in Table I), along with the values obtained by Levy from linewidth measurements.[5] Note that the reported values of τ are the average of a number of independent measurements taken for a given v_i'; the reported errors are one standard deviation.

The rates of vibrational predissociation $k(v_i',v_f')$ in Eq. (1) are taken as the inverse of the measured τ values (see Table I). The v_i' dependence of $k(v_i';v_f')$ is shown in Fig. 4 for both the I_2He and I_2Ne systems.

As with I_2Ne, [see (I)], we also observe rotational recurrences in the I_2He transients. These recurrences correspond to the nascent I_2^* (v_f'). For all of the transients recorded, the pump and probe lasers had parallel polarizations; the observed recurrences were in accord with this

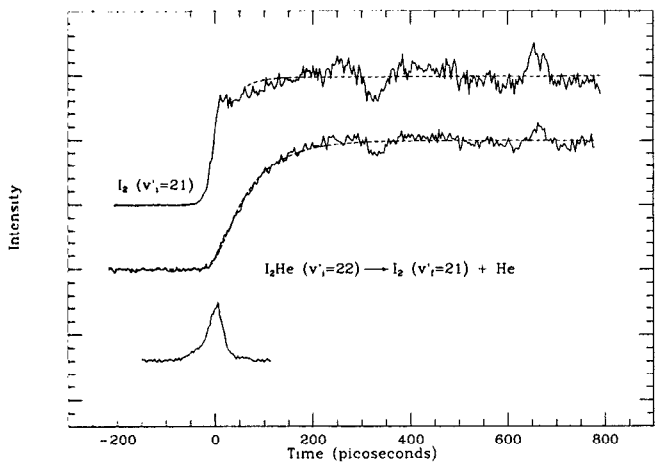

FIG. 1. A typical transient obtained for I_2He $v_i'=22/v_f'=21$ using the pump–probe/molecular beam methodology described in the text: (top) is a bare I_2 transient obtained for calibration; (middle) is a transient showing the predissociation (75±6 ps); and (bottom) is the visible cross correlation of the pump and probe lasers. The dashed lines show fits to an exponential rise function, convoluted with a Gaussian system response. For the bare iodine transients, these fits yield a very fast rise, determined by the laser pulse width. The rotational recurrences appearing on the predissociation transient are those of product I_2 in the $v_f'=21$ state and match those for the corresponding bare I_2 transient.

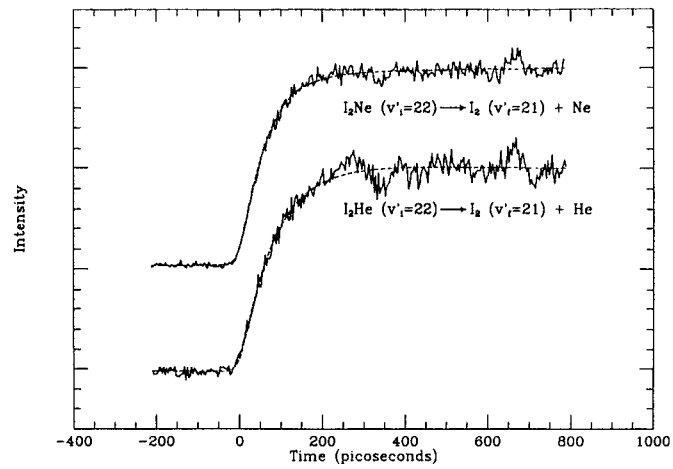

FIG. 2. Transients of I_2He and I_2Ne predissociation obtained when the same vibronic level ($v_i'=22$) is excited. The dashed lines show fits to an exponential rise function convoluted with a Gaussian system response; the vibrational predissociation lifetimes are found to be 75±6 ps for I_2He and 58±3 ps for I_2Ne.

arrangement.[8] The recurrences indicate that VP is sufficiently fast such that rotational coherence is retained in the products. Hence, there is a separation in the time scales of VP and the rotational motion, a point of interest which has been discussed in (I).

We have performed preliminary investigations of the vibrational predissociation rates in the I_2H_2 system. A transient is shown in Fig. 5 for $v_i'=17$ and $v_f'=16$. Levy and co-workers[9] reported a value of $D_e=74.4$ cm^{-1} for this cluster, which indicates a stronger bond than either the helium or neon bonds. The "energy-gap law"[6] (*vide infra*) would, therefore, predict a comparatively larger VP rate. This is the case; the VP lifetime for the I_2H_2 cluster for $v_i'=17$ is ~29 ps, while for I_2He or I_2Ne (Table I) the times are 128 and 126 ps. The 29 ps value is smaller than the 40 ps cross-correlation width of our laser system and if higher v_i' are studied, the lifetime is expected to decrease.

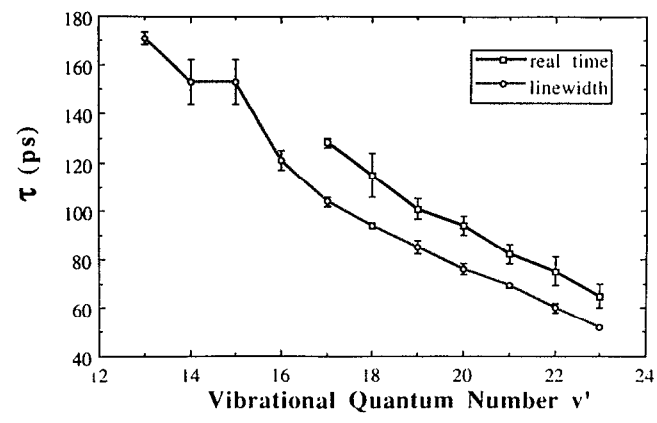

FIG. 3. The vibrational predissociation lifetimes of I_2He obtained from real-time studies (labeled by squares and a solid line), and from the linewidth measurements given in Ref. 5 (labeled by circles and a dashed line).

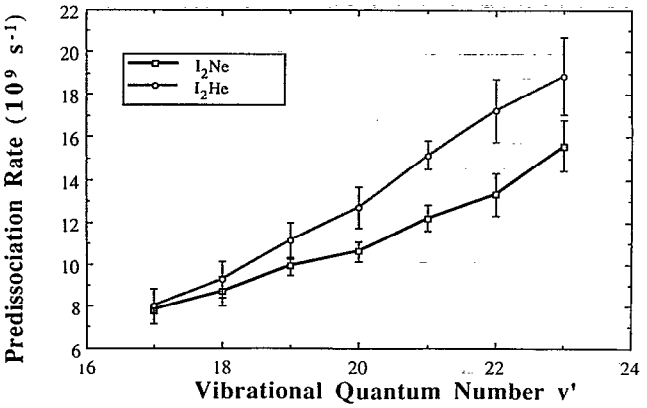

FIG. 4. The vibrational predissociation rates for I_2He and I_2Ne shown as a function of the vibrational level v_i' excited.

Further measurements of I_2H_2 VP rates will thus require shorter pulse laser systems.[2]

For I_2He, the results shown in Fig. 3 present a discrepancy upon comparison. The linewidth measurements give values of τ consistently shorter than the values obtained in our work; the linewidth was somehow broader than the intrinsic homogeneous VP width, a point we shall discuss below. As discussed in Ref. 5, the rotational spectrum was not completely resolved and corrections had to be made for overlapping rotational bands as well as for the Doppler broadening. Furthermore, the linewidth was obtained by fitting only the high frequency side of the R-branch head. When taking into account these deconvolutions, the discrepancy for I_2He [see (I) for the I_2Ne case] is perhaps expected. The two sets of data in Fig. 3 do indeed show the nonlinear dependence on v_i'.

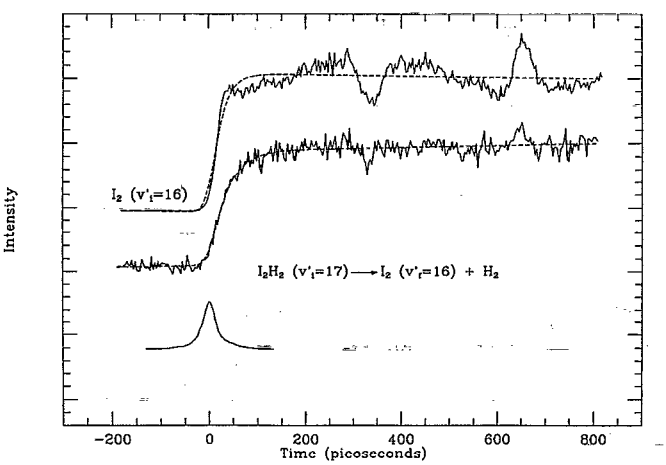

FIG. 5. The transient obtained for the vibrational predissociation of I_2H_2 when the cluster is excited to the $v_i' = 17$ vibrational level: (top) a bare iodine scan ($v_i' = 16$) which is taken for calibration; (middle) the transient showing the predissociation of the I_2H_2 cluster; (bottom) the cross correlation of the pump and probe laser pulses. The dashed lines are fits of the data to an exponential rise function convoluted with a Gaussian system response.

IV. DISCUSSION

A. Real-time vs linewidth measurements

As discussed previously,[1] homogeneous and inhomogeneous broadenings must be separated experimentally in order for linewidth measurements to give accurate rate values. Even if the transition is homogeneously broadened, pure dephasing[10] can lead to additional line broadening. In relatively small systems and near 0 K, however, one expects this effect to be minor. The more serious problem is a consequence of the following fact: If there is a dynamical process prior to the breakage of the bond, then the linewidth has no direct relationship to the rate of bond breakage. This effect has been shown for other vdW complexes of large molecules.[11]

For the case at hand, the small vdW clusters, the system may have discrete level structure (the equivalent of the so-called intermediate level structure in radiationless transition theory[12]), and one should address the question of preparation of the state. In a recent communication,[13] Halberstadt, Beswick, Roncero, and Janda (HBRJ) discussed the "discrepancy" between time-resolved vs frequency-resolved measurements of the VP rate in relation to the preparation question. In order to understand this problem it is useful to consider the nature of the dynamics in a VP process.

In the simplest approach, VP is the result of the coupling between the intramolecular (halogen stretch) and the intermolecular (vdW stretch) motion of the XBC cluster [here X denotes the vdW-bound rare gas atom (e.g., He), and BC represents the diatomic molecule [e.g., I_2)]. The coupling is between the zero-order states which are direct products of BC stretch wave functions and the vdW stretch wave functions. These zero-order states are not eigenstates of the full Hamiltonian. If we denote the BC stretch states by v', the bound vdW stretch states by l', and the vdW translational continuum states by ϵ', we have two types of zero-order states: $|v_i', l'\rangle$ and $|v_f', \epsilon'\rangle$. The vdW continuum states are indexed according to their translational kinetic energy, which is determined by the following relationship:

$$\epsilon' = E_{BC}(v_i') - E_{BC}(v_f') + \epsilon_{l'} . \qquad (2)$$

$E_{BC}(v')$ is the energy of the BC v' state and $\epsilon_{l'}$ is the vibrational energy of the vdW level $|l'\rangle$ corresponding to v_i'. For $l' = 0$, $\epsilon_{l'} = -D_0(XB)$ as shown in Table II. In Eq. (2) the effect of rotational excitation in nascent fragments has been neglected. VP arises essentially from the coupling between a zero-order bound state, e.g., $|v_i', 0\rangle$, and the quasidegenerate translational continuum $|v_f', \epsilon'\rangle$—a discrete state/continuum coupling which gives rise to a lifetime for the metastable resonance state (and homogeneous broadening). The zero-order picture for a system corresponding to I_2Ne or I_2He is shown in Fig. 6(a). The propensity rule for these systems is given by $v_f' = v_i' - 1$.

The system HBRJ considered[13] in their communication is Cl_2Ar in its electronic B state. In this case, the propensity rule for VP is from v_i' to $v_f' = v_i' - 2$. The schematic vdW potential diagram is shown in Fig. 6(b), and is

TABLE II. Definitions and expressions used in the theoretical calculations of vibrational predissociation rates.

D_{XB}	Potential well depth
$\omega_{XB}=\frac{1}{\mu_{XBC}}\left(\frac{\partial^2 U}{\partial Q^2}\right)Q_0$	Characteristic Morse frequency
$\mu_{XBC}=\frac{m_X(m_B+m_C)}{(m_X+m_B+m_C)}$	Reduced mass of the complex
$\alpha_{XB}=\omega_{XB}\left(\frac{\mu_{XBC}}{2D_{XB}}\right)^{1/2}$	Characteristic inverse length
$K_{XB}=\frac{2D_{XB}}{\hbar\omega_{XB}}$	Anharmonicity of the vdW Vibration
$\epsilon_{l'}=-D_{XB}+\hbar\omega_{XB}(l'+\frac{1}{2})\left(1-\frac{(l'+\frac{1}{2})}{2K_{XB}}\right)$ $=\frac{\hbar^2\alpha_{XB}}{2\mu_{XBC}}(K_{XB}-l'-\frac{1}{2})^2$	Energy of the bound vdW state $\|l'\rangle$
$\theta_{\epsilon'}=\frac{(2\mu_{XBC}\epsilon')^{1/2}}{\hbar\alpha_{XB}}=\frac{2(D_{XB}\epsilon')^{1/2}}{\hbar\omega_{XB}}$	Energy parameter
$N=(K_{XB}+\frac{1}{2})$	Number of bound states[a] in the Morse potential
$\mu_{BC}=\frac{m_B m_C}{(m_B+m_C)}$	Reduced mass of B–C
ω_{BC}	Frequency of the B–C stretch vibration
$K_{BC}=\frac{\omega_{BC}}{2(\omega x_e)_{BC}}$	Anharmonicity of the B–C stretch vibration

[a]The calculated value of N should be rounded off to an integer.

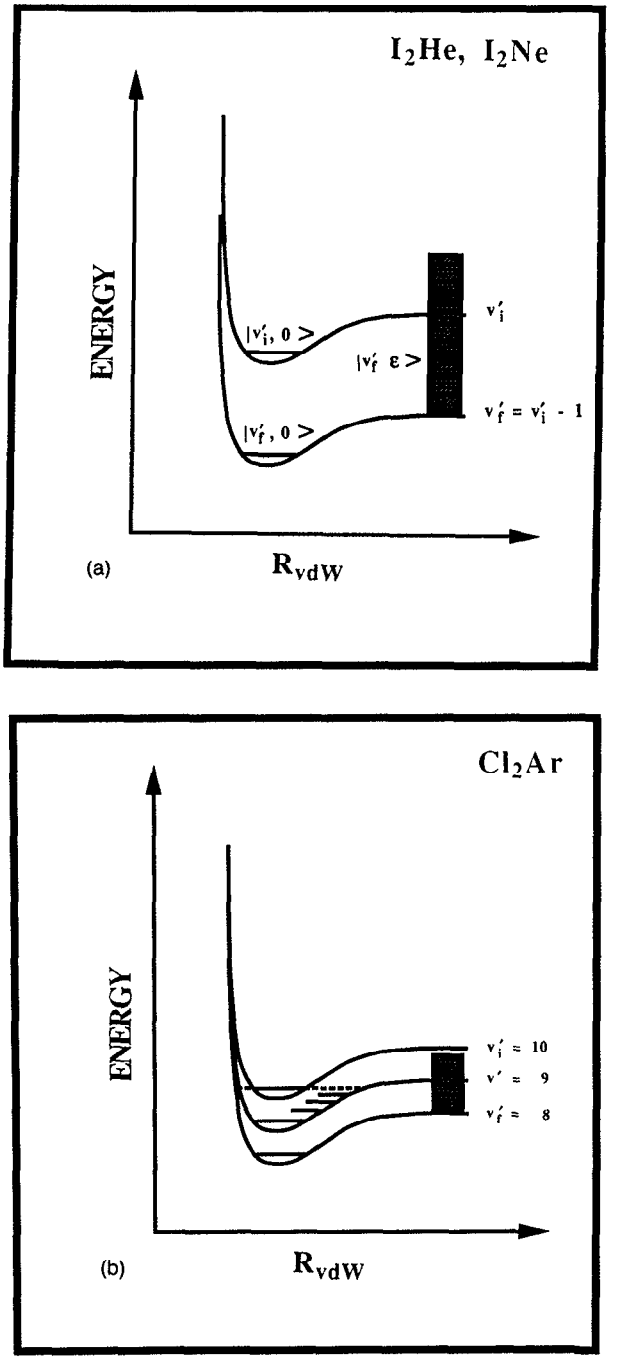

FIG. 6. (a) A schematic of the vdW potential for vibrational predissociation in the systems I_2He and I_2Ne along the intermolecular coordinate R_{vdW}. The corresponding I_2 stretch quantum numbers and the relevant zero-order states are given. The vdW translational continuum corresponding to v'_f is shown as a block. For details, see the text. (b) Same as (a) but for Cl_2Ar. The zero-order states are not explicitly labeled. For details, see the text.

to be contrasted with the corresponding picture for I_2He and I_2Ne in Fig. 6(a). HBRJ found that at $v'_i = 10$, the ground state vdW vibration is strongly coupled to energetically high lying (discrete) vdW vibrations of the $v'=9$ Cl_2 stretch level in Cl_2Ar. These states then, in turn, couple to the vdW translational continuum of the Cl_2 $v'_f = 8$ stretch level. The authors proposed a two-step mechanism, shown in Fig. 7, which is adopted in part from Ref. 14. IVR in the sparse limit is assumed to be the first step. Dissociation from the levels obtained by mixing the zero-order light state $|s\rangle$ (direct product of the Cl_2 stretch ($v'_i = 10$) and the corresponding vdW ground state) with the dark states $\{|k\rangle\}$ (direct products of the Cl_2 stretch ($v'=9$) with corresponding high lying discrete vdW states) to the translational continuum $\{|\epsilon'\rangle\}$ of the vdW states of the Cl_2 stretch $v'_f = 8$ occurs as the second step (VP1). HBRJ assumed that the light state predominantly couples to the dark states, which are in turn weakly coupled to the continuum; thus the direct coupling between the light state and the continuum (VP2) may not be observed (Fig. 7). This is the classic IVR problem and the preparation of the state is important for observation of the dynamics (phase-shifted quantum beats and decay).[15]

As noted by the authors, and as discussed previously,[15] a frequency domain experiment employing a cw laser with a very narrow bandwidth prepares the system in a molecular eigenstate, and not in a zero-order state. The linewidth Γ of this "scattering resonance" reflects the predissociation lifetime τ of a mixed state ($|s\rangle$ and $\{|k\rangle\}$) as the laser bandwidth is too small to observe IVR effects. The connection of τ to Γ is given by

$$\tau=\frac{\hbar}{\Gamma}. \tag{3}$$

A time-resolved experiment with a coherent bandwidth prepares the system in a nonstationary (coherent)

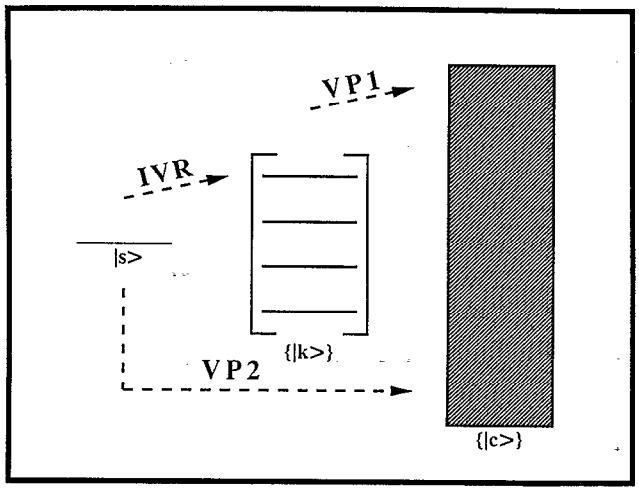

FIG. 7. A schematic of the coupling schemes for the two step mechanism of VP. For details, see the text.

superposition of molecular eigenstates (e.g., in a zero-order state, $|s\rangle$). The $|s\rangle$ state then evolves to reveal the dynamics of both IVR and VP. In the case discussed by HBRJ, such a time-resolved experiment, spanning an energy band that includes at least one dark state, would give a combination of an IVR "rate" (with possible recurrences[15] in the sparse limit) and a VP rate, VP1. Thus if the rises are fitted to a single exponential, an effective rate, which is slower than the pure VP1 rate, may result. As the VP rates we reported for I_2Ne in Paper (I) (and also those for I_2He reported in this contribution) are consistently smaller than those obtained from linewidth measurements, HBRJ concluded that I_2Ne might undergo IVR in the sparse limit, similar to Cl_2Ar.

However, inspection of Fig. 6(a) shows that in our case the initial state $|s\rangle$ can only couple to the vdW translational continuum according to the propensity rule valid for I_2Ne and I_2He, i.e., $v_f' = v_i' - 1$. The initial state prepared by the short laser pulse thus directly couples to the continuum and the only possible route for VP in I_2Ne and I_2He is the VP2 shown in Fig. 7. This is also consistent with the fact that (on our time scale) we do not observe quantum beats which may arise if IVR is in the sparse limit and precedes VP. Also, as discussed below, the energy-gap law (in relative terms) holds at least qualitatively for both I_2He and I_2Ne. A violation of the energy-gap law was, however, observed in Cl_2Ar (see Ref. 13) for which the propensity rule is $v_f' = v_i' - 2$.

It is thus concluded that our real-time results give the VP rates and the linewidth measurements provide an upper limit, because of the reasons discussed above and in (I). It should, however, be noted that due to the good resolution of the rotational bands and the careful deconvolution[5] for I_2He, the linewidths are in discrepancy to $\sim 30\%$ and the v_i' dependence is still apparant. For more complex systems, I_2X_n of Paper (III), the situation is very different, as the dynamics are controlled by more than one channel.

B. Comparison with the energy-gap law (EGL)

In order to rationalize the VP rates of triatomic vdW clusters, some simplifying rules have been devised theoretically. In particular, the EGL, derived by Beswick and Jortner,[6] and the momentum-gap law, derived by Ewing,[16] have been of considerable value in offering an understanding of the behavior of VP rates with v_i'. Beswick and Jortner[6] derived the EGL from an analytic expression obtained by (approximately) treating VP within the Fermi golden rule approach, as discussed in (I). They based their pertubative diabatic distorted wave (DDW) framework on such a Fermi golden rule approach. When assuming a collinear configuration of the cluster and linearizing the vdW Morse potential with respect to the intramolecular coordinate, they obtained an expression for the halfwidth $\Gamma/2$. In (I), we discussed their approach and the dependence of Γ on the intramolecular (iodine) and intermolecular (iodine–rare gas) potentials. Γ is expressed as

$$\Gamma = \frac{\pi}{4}\hbar\omega_{BC}\frac{\mu_{XBC}}{\mu_{BC}}v_i'\frac{(2K_{BC}-2v_i'+1)(2K_{BC}-2v_i'-1)}{2K_{BC}(2K_{BC}-v_i')} \otimes \frac{\sinh(2\pi\theta_{\epsilon'})}{\cos^2(\pi K_{XB})+\sinh^2(\pi\theta_{\epsilon'})}\,|\tilde{\Gamma}(K_{XB}+\tfrac{1}{2}-i\theta_{\epsilon'})|^2 \otimes \frac{2K_{XB}-2l'-1}{l'!\tilde{\Gamma}(2K_{XB}-l')}, \tag{4}$$

where $\tilde{\Gamma}$ denotes the gamma function. The symbols used in this equation and in the following expressions are explained in Table II, and detailed in (I). BC denotes the halogen molecule and X the vdW-bound rare gas atom. The vdW potential is assumed to be of Morse type. For large values of $\theta_{\epsilon'}$ Eq. (4) can be simplified to give[6]

$$\Gamma = 2\pi^2\hbar\omega_{BC}\frac{\mu_{XBC}}{\mu_{BC}}v_i'\frac{(2K_{BC}-2v_i'+1)(2K_{BC}-2v_i'-1)}{2K_{BC}(2K_{BC}-v_i')} \otimes \frac{N-l'-1}{l'!(2N-l'-1)!}\theta_{\epsilon'}^{2N-1}\exp[-\pi\theta_{\epsilon'}]. \tag{5}$$

In the limit when $\theta_{\epsilon'} \gg 1$ (by orders of magnitude) and $v_i' < K_{BC}$, the exponential in Eq. (5) dominates and the EGL can be expressed as

$$\Gamma \propto v_i'\exp[\gamma v_i'], \tag{6}$$

where

$$\gamma = \pi\frac{(\mu_{XBC}\hbar\omega_{BC}/2)^{1/2}}{K_{BC}\hbar\alpha_{XB}}. \tag{7}$$

With the vdW potential parameters obtained by Levy and co-workers from their spectroscopic work,[17] we calculated $\theta_{\epsilon'}$ and obtained, for $v_i' = 20$ (electronic B state), $\theta_{\epsilon'}(I_2He) = 10.36$ and $\theta_{\epsilon'}(I_2Ne) = 3.54$ [cp. (I)]. For both systems, $\theta_{\epsilon'}$ is clearly greater than one, but only for I_2He does the approximation made in order to apply Eq. (5) (i.e., $\theta_{\epsilon'} \gg 1$), appear to be justified. This is borne out by actually calculating the VP time using Eqs. (4) and (5). For I_2He ($v_i' = 20$), we obtain 1.5 μs from Eq. (4) and 23

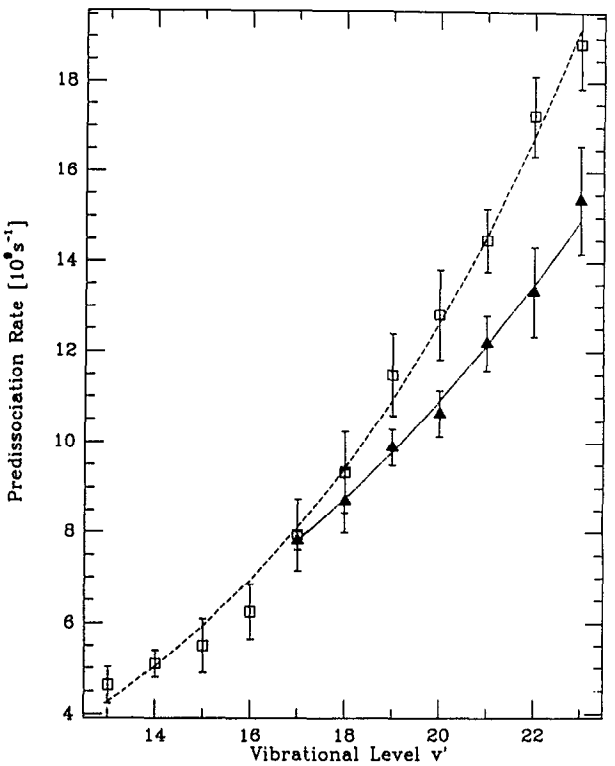

FIG. 8. Theoretical fits of the real-time VP rates to the energy-gap law expressed in Eq. (8). The experimental data and the reported error bars are also shown. The open squares are the data for I_2Ne, and the filled triangles are those for I_2He. The vibrational levels on the abscissa correspond to v_i'.

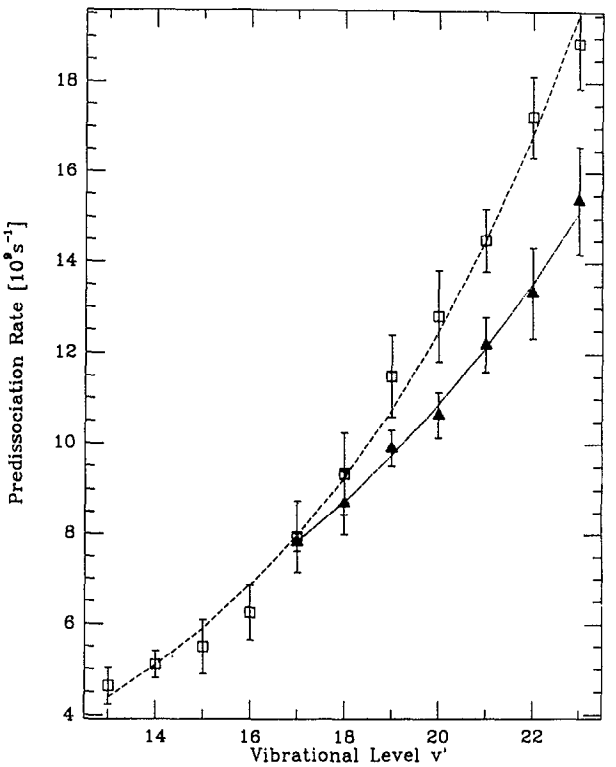

FIG. 9. Same as in Fig. 8 except that the fits are made to the simple exponential function given in Eq. (9).

μs as a result of the approximation in Eq. (5). For I_2Ne ($v_i' = 20$), Eq. (4) leads to 2.6 ps and Eq. (5) gives 2.8 ns [cp. (I)]. The results for I_2He are closer in value to each other than those for I_2Ne, perhaps justifying approximation (5) for the He system.

In order to compare the v_i' dependence of the experimental VP rates with the behavior predicted by the EGL, we fitted our results to the functional form

$$\frac{1}{\tau} \propto v_i' \exp[\gamma v_i']. \tag{8}$$

For I_2He, this yields $\gamma=0.0579$ which corresponds to a Morse length parameter of $\alpha=1.81$ Å^{-1} and for I_2Ne, $\gamma=0.0936$, corresponding to $\alpha=2.43$ Å^{-1} [cp. (I)]. The fits, together with our experimental data, are shown in Fig. 8. The fits do indeed show the expected trend $\alpha(\text{He}) < \alpha(\text{Ne})$. This expectation is based on the *effective* Morse potential parameters derived by Levy and co-workers from the spectroscopic work on I_2He and I_2Ne in the B state.[17] We note that while the overall behavior is correctly described by the fits to Eq. (8), the absolute magnitudes of the rates derived by the EGL [Eqs. (4) and (5)] are orders of magnitudes different from experiments, as shown above.

We also attempted fits to the simpler exponential expression

$$\frac{1}{\tau} \propto \exp[\gamma v_i']. \tag{9}$$

These fits lead to $\gamma=0.1098$ corresponding to $\alpha=0.95$ Å^{-1} for I_2He, and to $\gamma=0.1493$ corresponding to $\alpha=1.52$ Å^{-1} for I_2Ne [cp. (I)]. The fits are shown in Fig. 9. The change in α between I_2Ne and I_2He is still the same. Thus it appears that the intermolecular term (exponential) dominates the behavior of the v_i' dependence.

In order to compare the v_i' behavior in our data with those obtained from linewidth measurements, we invoked the functional form for I_2He used by Levy and co-workers[5]

$$\frac{1}{\tau} = A(v_i')^2 + B(v_i')^3. \tag{10}$$

The values obtained by Levy and co-workers, fitting the halfwidths of the observed bands (not $1/\tau$), were $A=5.55\times10^{-4}$ and $B=1.74\times10^{-6}$, which when translated into Eq. (10) (i.e., $1/\tau$ instead of $\Gamma/2$) give $A=2.09\times10^7$ and $B=6.555\times10^5$. For the purpose of a more accurate comparison, we refitted the $1/\tau$ data deduced from Ref. 5 using a Marquardt nonlinear least-squares fit algorithm.[7] Instead of the above values, we arrived at $A=2.646\times10^7$ and $B=3.969\times10^5$. Using a SIMPLEX routine,[18] we reproduced these results again. Replacing the correct (error-weighted) χ^2 by the sum of squared differences between the observed and the calculated data, however, led to the same results that Levy and co-workers obtained. Thus it seems that the fits that these authors performed were unweighted, leading to slightly different results. In order to keep our compari-

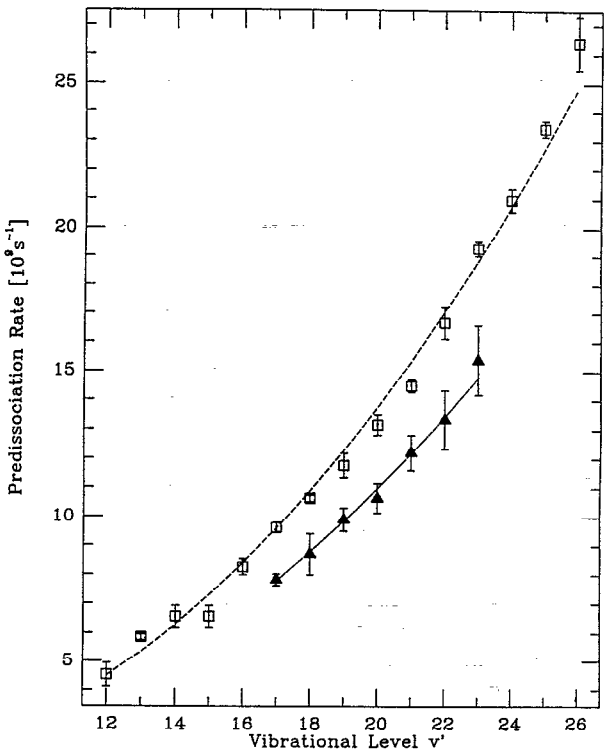

FIG. 10. Theoretical fits of the real-time VP rates and the linewidth deduced VP rates (Ref. 5) for I_2He to Eq. (10). The experimental data together with reported error bars are also given. The real-time data are shown as filled triangles and the linewidth data as open squares. The vibrational levels on the abscissa correspond to v_i'.

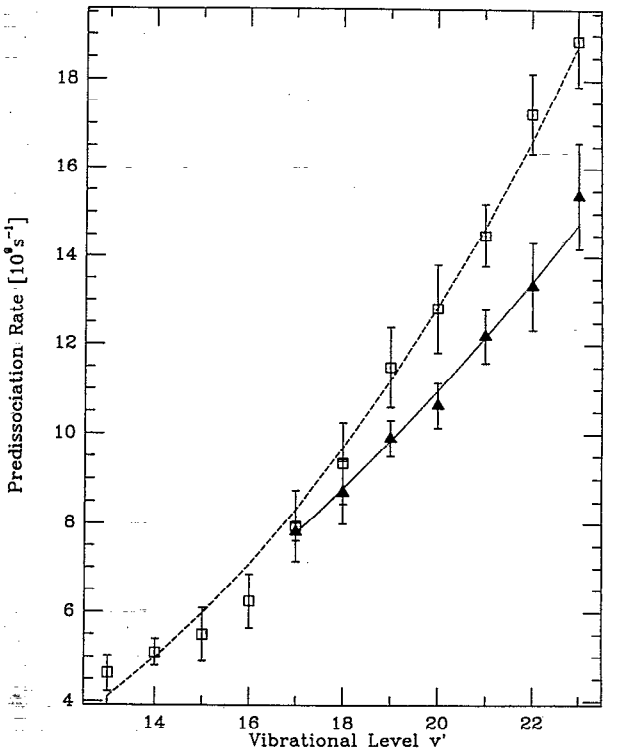

FIG. 11. Theoretical fit of the real-time VP rates for I_2Ne to Eq. (10), together with those corresponding to the I_2He results. The experimental data together with the reported error bars are also shown. Filled triangles denote the I_2He data and open squares the I_2Ne data. The vibrational levels on the abscissa correspond to v_i'.

son consistent, we will only compare with the weighted fits, i.e., $A=2.646\times10^7$ and $B=3.969\times10^5$.

From our experimental data of the VP of I_2He, we obtained $A=2.423\times10^7$ and $B=1.594\times10^5$. A comparison of the two fits together with the corresponding experimental data is shown in Fig. 10. It appears that in our fits, the quadratic term dominates with respect to the cubic term, and this is slightly different from the fits to the data of Ref. 5, when considering the relative A/B values. This may be due to the fact that the latter data were obtained for vibrational levels up to 26. If the data for levels 12–16 and 24–26 are discarded, the coefficient for the cubic term becomes even higher than when fitting to the full data set; the quadratic term is nearly equal to that in our data. Thus the VP rates given in Ref. 5 still appear to rise a little faster with respect to v_i' than ours, but the differences are minor. It is concluded that while the linewidth data lead to consistently larger VP rates than the real-time results, both show a very similar nonlinear behavior with respect to v_i'. An analogous fit of our real-time data of I_2Ne (v_i' = 13–23) gives $A=9.890\times10^7$ and $B=1.111\times10^7$ and is depicted in Fig. 11. These results show that the VP rates of I_2Ne rise (with v_i') faster than those of I_2He, as expected from theory.

This faster rise for the I_2Ne system cannot, however, be explained only by the simple reduced mass considerations (for discussion see Ref. 19). In order to observe the effect of the mass change, the molecular parameters which characterize the dimensionless parameter $\theta_{\epsilon'}$ (α and ϵ'), given above and in Table II, must not change appreciably when going from the I_2He system to the I_2Ne system. In addition, the effect of the reduced mass appearing in the pre-exponential factor [see Eq. (5)] should be negligible. If these conditions and the assumptions leading to Eq. (5) (e.g., collinear configuration of the cluster) are met, then it is predicted[19] that the VP rate, at least for high quantum numbers l', becomes larger when the mass of the rare gas atom is decreased. This is exactly opposite to the observed behavior within the range of v_i' quantum numbers covered in our experiments. The contradiction is not too surprising as the potential parameters change appreciably when going from the I_2He to the I_2Ne system. However, a logarithmic correlation between the VP time and the parameter $\theta_{\epsilon'}=(2\mu_{XBC}\epsilon')^{1/2}/\alpha_{XB}\hbar$ itself, as proposed by Ewing[16] (momentum-gap law), appears to point along the right direction, although the actual values of the correlation are not reproduced: With the values for α and D_0 obtained by Levy and co-workers[17] [$\alpha(I_2He)=0.41$ Å^{-1}, $D_0(I_2He)=14.2$ cm^{-1}; $\alpha(I_2Ne)=1.5$ Å^{-1}, $D_0(I_2Ne)=66$ cm^{-1}) we calculate for $v_i'=20$ that $\theta_{\epsilon'}(I_2He)$ is about 2.9 $\theta_{\epsilon'}(I_2Ne)$ (*vide supra*), whereas $\ln[\tau_{VP}(I_2He)]=1.04\ln[\tau_{VP}(I_2Ne)]$. When using $\alpha(I_2He)=1.14$ Å^{-1}, a value used in most theoretical calculations for the atom–atom (I–He) Morse potential (*vide infra*), and keeping the val-

ues of all the other parameters the same, one obtains a value of 1.04 instead of 2.9.

C. Comparison with classical and quantum calculations

In (I), we made the comparison of our experimental results with numerical data, obtained by different groups, for I_2Ne. Here we focus on the I_2He system. Calculations of the VP rates of I_2He in its electronic B state have been performed for collinear and nonlinear cluster geometries. As the T-shaped configuration of I_2He is the most likely one,[4] we will only consider the numerical results which were obtained for a nonlinear configuration.

The results of any calculation addressing VP of vdW systems crucially depend on the parameters used for the assumed sum of two halogen atom–rare gas atom Morse potentials (the form of the long range part of the vdW potential itself does not appear to be too important[20]). These Morse potential parameters should be compared to the *effective* ones deduced by Levy and co-workers;[17] from fits of spectroscopic data they obtained the following parameters for a Morse potential (I_2He, B state): D_{XB} $=13.6$–14.8 cm^{-1} and an *effective* $\alpha=0.4$–0.42 $Å^{-1}$. In comparing these α values with those used in theory (most often $\alpha_{XB}=1.14$ $Å^{-1}$ and $D_{XB}=18$ cm^{-1}; values which fitted the results of close coupling calculations[6] best to the rates deduced in Ref. 5, particularly for higher v_i'), one has to keep in mind the difference: The α values used in theory are those for each of the two atom–atom potentials, whereas the values obtained from experiment[17] are for a single *effective* Morse potential along the vdW stretch coordinate.

The first calculation which employed a fixed T-shaped configuration was performed by Beswick and Jortner in 1978.[21] They calculated VP rates within the close coupling framework, i.e., by numerically solving the coupled differential equations obtained by invoking a basis set expansion in the Schrödinger equation and calculating the appropriate scattering matrix elements. With $D_{XB}=7$ cm^{-1} and $\alpha=1.25$ $Å^{-1}$, they obtained a VP time of ~ 835 ps for v_i' $=20$ ($l'=0$), whereas changing D_{XB} to 25 cm^{-1} gave a value of 67 ps, closer in magnitude to our experimental result of 94 ps. The I_2 stretch vibration was treated in a harmonic approximation, and the calculated results depended on the potential parameters used.

Beswick, Delgado-Barrio, and Jortner[20] included the anharmonicity of the I_2 stretch vibration into their close coupling formalism. They obtained for $v_i'=20$ ($l'=0$, D_{XB} $=7$ cm^{-1}, $\alpha=1.24$ $Å^{-1}$) a VP time of ~ 240 ps, thus drastically reducing the above result of 835 ps obtained with the same parameters but without the anharmonicity of the intramolecular mode. Changing D_{XB} to 13 cm^{-1} led to a VP time of 80 ps, also close to our experimental result of 94 ps.

In 1980, Beswick and Delgado-Barrio[22] included a treatment of rotations into the DDW scheme. The rotations were treated within the infinite order sudden approximation (IOSA). From Figs. 3 and 4 of Ref. 22 we can extract the following results for $v_i'=20$ ($l'=0$): With D_{XB} $=7$ cm^{-1} and $\alpha=1.24$ $Å^{-1}$, the VP time was calculated to be ~ 775 ps; with $D_{XB}=18$ cm^{-1} and $\alpha=1.14$ $Å^{-1}$, the result was about 265 ps. These authors also calculated the rotational excitation of the fragment I_2 during VP and found it to be very minor, indicating a V–T process.

Recently, a three-dimensional quantum wave packet calculation of VP in I_2He was reported by Zhang and Zhang.[23] They also found that while the rotational state distribution of the nascent I_2 is independent of v_i' and is restricted to low rotational levels, the rates become much smaller when compared with the results of the two-dimensional (nonrotating, fixed T-shaped geometry) calculations. The Morse potential parameters the authors used were $D_{XB}=18$ cm^{-1} and $\alpha=1.24$ $Å^{-1}$. From Fig. 1 of Ref. 23, a VP time of about 115 ps can be extracted (three-dimensional) for $v_i'=20$, which is close to our experimental value of 94 ps.

In order to facilitate the computational effort and to be able to treat larger systems, quasiclassical trajectory methods were introduced for the calculation of VP times; a classical approximation does not seem to be appropriate for this inherently quantum mechanical process since I_2 gives the energy in a quantized (not continuous) form. Nevertheless, a quasiclassical trajectory calculation by Delgado-Barrio and co-workers[24] was performed for I_2He ($v_i'=23$, $l'=0$, no bending excitation, overall angular momentum $J=0$) and led to a VP time of about 65 ps (extracted from Fig. 2 of Ref. 24). They used $D_{XB}=18$ cm^{-1} and $\alpha=1.14$ $Å^{-1}$. This result is identical with the VP time we measured for $v_i'=23$.

Recently, statistical methods based on quasiclassical trajectory calculations were developed by Davis, Gray, Rice, and co-workers.[25–30] Within the framework of these methods, which invoke concepts from nonlinear dynamics, "intermolecular bottlenecks" in phase space are defined as dynamic transition states of fragmentation. The rates of VP are obtained by calculating the flux of phase points across the intermolecular bottleneck. These methods work better at higher v_i' values. For low v_i' levels, the rates across intramolecular bottlenecks, which lie within the intermolecular ones, gain importance as they become rate limiting.

Davis and Gray[26] calculated the VP rates of T-shaped I_2He (two coordinate system) by considering the flux of phase points across the exact intermolecular bottleneck. Using $D_{XB}=18$ cm^{-1}, $\alpha=1.14$ $Å^{-1}$ they obtained, for v_i' $=20$, a VP time of 14 ps. A numerical (classical trajectory) simulation led to a value of 31 ps. Including one intramolecular bottleneck, they obtained a statistically calculated VP time of 31 ps which matches the result of the numerical simulation.

The alternative RRKM (ARRKM) method[27] considers an approximate intermolecular bottleneck. Gray, Rice, and Davis calculated the VP time of T-shaped I_2He (Ref. 28) for $v_i'=20$; using $D_{XB}=18$ cm^{-1}, $\alpha=1.14$ $Å^{-1}$, they obtained 6.5 ps. With a calculation of the flux of phase points across the approximate intermolecular bottleneck, they obtained a VP time of 8 ps. These results appeared to be in fairly good agreement with those obtained employing the exact intermolecular bottleneck. Inclusion of rotations

TABLE III. Theoretical predictions of the vibrational predissociation lifetime of I_2He ($v_i' = 20, J' = 0$). (The experimental value from this work is 94±4 ps.)

Method[a,b]	D_{XB} (cm^{-1})	α_{XB} ($Å^{-1}$)	τ(ps)	2D/3D[c]	Ref.
Close coupling (I_2 stretch is treated harmonically)	7	1.25	835	2D	21
	25	1.25	67	2D	
Close coupling (I_2 stretch is treated anharmonically)	7	1.24	240	2D	20
	13	1.24	80	2D	
DDW+IOSA	7	1.24	775	3D	22
	18	1.14	265	3D	
Quantum wave packet	18	1.14	115	3D	23
Classical trajectory	18	1.14	65(v_i'=23)	3D	24
Classical trajectory	18	1.14	31	2D	26
Flux across exact intermolecular bottleneck	18	1.14	14	2D	
ARRKM	18	1.14	6.5	2D	28
Flux across approximate intermolecular bottleneck	18	1.14	8	2D	
ARRKM	18	1.14	3.5	3D	
MRRKM (intermolecular bottleneck)	18	1.14	13.5	2D	30
	18	1.14	41	3D	
MRRKM (intermolecular bottleneck)	18	1.14	20	2D	
MRRKM (intermolecular and intramolecular bottleneck)	18	1.14	22	2D	
	18	1.14	62	3D	

[a]Abbreviations in this table are explained in the text.
[b]Calculations according to Eq. (4)—EGL—in the text are not included in the table as this equation was derived analytically for a linear complex. As shown in the text, when using the effective α parameter from Ref. 17, τ for $v_i' = 20$ is 1.5 μs.
[c]2D corresponds to a fixed T-shaped geometry not allowing for rotational or bending motion, 3D differs from 2D by inclusion of rotational (and bending) motion.

into the ARRKM method leads, however, to a considerable deviation of the results when compared with classical trajectory calculations and experimental data. For $v_i' = 20$, keeping the overall angular momentum $J=0$, Gray, Rice, and Davis calculated a VP time of 3.5 ps.[27]

Very recently, Zhao and Rice[29,30] extended the ARRKM method by defining rovibrational state dependent bottlenecks which took into account the actually excited initial state. The method emerging from these considerations has been termed modified RRKM (MRRKM) theory. Using the same parameters, i.e., $D_{XB}=18$ cm^{-1}, $\alpha=1.14$ $Å^{-1}$, they performed several MRRKM calculations[30] for both I_2He and I_2Ne. For $v_i' = 20$, the VP time for I_2He (when only the intermolecular bottleneck is accounted for and the geometry is fixed, nonrotating, and T shaped) was calculated to be 13.5 ps. Allowing for rotations, but keeping the overall angular momentum $J=0$, these authors calculated a VP time of 41 ps. They also calculated the VP time considering only the intramolecular bottleneck and keeping the cluster in a fixed T-shaped configuration and obtained 20 ps. Including the intermolecular bottleneck yielded 22 ps. Finally, allowing for rotation and keeping $J=0$ they obtained, taking into consideration the intra- and intermolecular bottlenecks, a VP time of 62 ps, which is closer to the experimental value of 94 ps.

As noted above, the influence of rotations is significant. Even though the rotational excitation of the departing I_2 fragment is negligible, the inclusion of rotations has a profound effect on the calculation of the absolute rates. It appears that VP rate calculations have to take into account such effects. The influence of overall rotations on microcanonical rates has been observed experimentally[31] and cal-

culated theoretically[32] in other cases where a chemical bond is broken to form two fragments (e.g., NCNO→NC +NO). The effect is more dramatic near threshold energies. Further quantum calculations using the wave packet approach are underway[33] and it would be interesting to include the effect of rotations. Also, it seems worthwhile to study in depth the applicability of classical models to these systems where quantum effects are expected to have influence on the dynamics.

Table III summarizes the comparison of results of all theories available and the experimental results reported here, focusing on $v_i' = 20$ for the above discussion.

V. CONCLUSIONS

The present contribution addressed two main issues concerning the picosecond dynamics of vibrational predissociation (VP) in small van der Waals (vdW) clusters. First, by studying the VP of I_2He in real-time, we were able to present results for a rare example where linewidth deduced and real-time VP rates were directly compared for the same system and for the same range of quantum states excited. From this comparison, we found that the linewidth deduced data led to consistently higher rate values. For I_2Ne, the discrepancy is more pronounced and for larger clusters [Paper (III)] the linewidth cannot separate the dynamics of the two VP pathways. These results were discussed in relation to the origin of the line broadening and to the question of preparation of the state. The VP rate dependence on the quantum number of the I_2 stretch vibration in I_2He was measured and both methods display the highly nonlinear behavior.

Second, we have compared the experimental results on I_2He and I_2Ne with a variety of theoretical approaches (classical, quantum, and semiclassical) in an attempt to understand the forces controlling the dynamics. Theories for calculating VP rates of small vdW clusters are quite advanced and it is important to critically examine the predictions of the different approaches. The repulsive force of the potential of the vdW interaction plays a key role and the theoretical results depend crucially on such input parameters.

While theories agree with each other on the quantum state dependence of the rates, they differ in their prediction of the absolute rate values by orders of magnitude. The dependence of the state-to-state rates on the initial vibrational quantum number can be understood using the energy-gap law as well as a number of other numerical methods. The energy-gap law, however, does not provide the absolute rate. A simple model[34] can deduce such dependencies by considering the repulsive force of the potential in the reverse problem of T–V transfer (full collision).

Methods based on classical concepts are now used to calculate VP rates. Why methods such as the MRRKM by Rice and co-workers[29,30] deduce rates in quantum systems (defined by the initial quantum number of the vibrations and their discrete energies) is an interesting question. If generalized and tested against quantum calculations, these methods could prove useful for larger systems with increased numbers of degrees of freedom, a transition we are making in Paper (III)[35] of this series, where n is greater than one for I_2He_n and I_2Ne_n.

ACKNOWLEDGMENT

This work was supported by a grant from the National Science Foundation (DMR).

[1] D. M. Willberg, M. Gutmann, J. J. Breen, and A. H. Zewail, J. Chem. Phys. **96**, 198 (1992).
[2] L. Khundkar and A. H. Zewail, Annu. Rev. Phys. Chem. **41**, 15 (1990), and references therein.
[3] D. H. Levy, Adv. Chem. Phys. **47**, part I, 323 (1981), and references therein.
[4] R. E. Smalley, L. Wharton, and D. H. Levy, J. Chem. Phys. **68**, 671 (1978).
[5] K. E. Johnson, L. Wharton, and D. H. Levy, J. Chem. Phys. **69**, 2719 (1978).
[6] J. A. Beswick and J. Jortner, Adv. Chem. Phys. **47**, part I, 363 (1981), and references therein
[7] P. R. Bevington, *Data Reduction and Error Analysis for the Physical Sciences* (McGraw-Hill, New York, 1969), p. 204.
[8] D. M. Willberg, J. J. Breen, M. Gutmann, and A. H. Zewail, J. Phys. Chem. **95**, 7136 (1991).
[9] J. E. Kenny, T. D. Russell, and D. H. Levy, J. Chem. Phys. **73**, 3607 (1980).
[10] A. H. Zewail, Acc. Chem. Res. **13**, 360 (1980).
[11] D. M. Semmes, J. S. Baskin, and A. H. Zewail, J. Chem. Phys. **92**, 3359 (1990).
[12] For a review, see J. Jortner and S. Mukamel, in *The World of Quantum Chemistry*, edited by R. Daudel and B. Pullman (Reidel, Dordrecht, 1976), p. 205.
[13] N. Halberstadt, J. A. Beswick, O. Roncero, and K. C. Janda, J. Chem. Phys. **96**, 2404 (1992).
[14] W. R. Gentry, in *Structure and Dynamics of Weakly Bound Molecular Complexes*, NATO ASI series, edited by A. Weber (Reidel, Dordrecht, 1987), p. 467.
[15] P. M. Felker and A. H. Zewail, Adv. Chem. Phys. **70**, part I, 265 (1988).
[16] (a) G. E. Ewing, J. Chem. Phys. **71**, 3143 (1979); (b) **72**, 2096 (1980); (c) Faraday Discuss. Chem. Soc. **73**, 325, 402 (1982); (d) J. Phys. Chem. **90**, 1990 (1986).
[17] J. A. Blazy, B. M. DeKoven, T. D. Russell, and D. H. Levy, J. Chem. Phys. **72**, 2439 (1980).
[18] This program was based on an algorithm from M. Caceci and W. P. Cacheris, BYTE May, 340 (1984).
[19] J. A. Beswick and J. Jortner, J. Chem. Phys. **68**, 2277 (1978).
[20] J. A. Beswick, G. Delgado-Barrio, and J. Jortner, J. Chem. Phys. **70**, 3895 (1979).
[21] J. A. Beswick and J. Jortner, J. Chem. Phys. **69**, 512 (1978).
[22] J. A. Beswick and G. Delgado-Barrio, J. Chem. Phys. **73**, 3653 (1980).
[23] D. H. Zhang and J. Z. H. Zhang, J. Phys. Chem. **96**, 1575 (1992).
[24] G. Delgado-Barrio, P. Villerreal, P. Mareca, and G. Albelda, J. Chem. Phys. **78**, 280 (1983).
[25] M. J. Davis, J. Chem. Phys. **83**, 1016 (1985).
[26] M. J. Davis, and S. K. Gray, J. Chem. Phys. **84**, 5389 (1986).
[27] S. K. Gray, and S. A. Rice, Faraday Discuss. Chem. Soc. **82**, 307 (1986).
[28] S. K. Gray, S. A. Rice, and M. J. Davis, J. Phys. Chem. **90**, 3470 (1986).
[29] M. Zhao, and S. A. Rice, J. Chem. Phys. **96**, 3542 (1992).
[30] M. Zhao, and S. A. Rice, J. Chem. Phys. **96**, 6654 (1992).
[31] L. R. Khundkar, J. L. Knee, and A. H. Zewail, J. Chem. Phys. **87**, 77 (1987).
[32] J. Troe, Ber. Bunsenges. Phys. Chem. **92**, 242 (1988).
[33] S. K. Gray (private communication).
[34] D. M. Willberg, M. Gutmann, E. E. Nikitin, and A. H. Zewail, Chem. Phys. Lett. (in press).
[35] M. Gutmann, D. M. Willberg, and A. H. Zewail, J. Chem. Phys. **97**, 8048 (1992).